



OPEN ACCESS

EDITED BY

Victor H. Bustamante, National Autonomous University of Mexico, Mexico

REVIEWED BY

Roberto Rosales-Reves. National Autonomous University of Mexico, Yasmine Hasanine Tartor, Zagazig University, Egypt

*CORRESPONDENCE

Francesca Di Bartolomeo

RECEIVED 16 May 2025 ACCEPTED 25 September 2025 PUBLISHED 16 October 2025

Eidsaa M, Sharma A, Janasch M, Kuch A, Skoczyńska A and Di Bartolomeo F (2025) Proteomic landscape of imipenem resistance in Pseudomonas aeruginosa: a comparative investigation between clinical and control strains. Front, Cell. Infect. Microbiol. 15:1623154. doi: 10.3389/fcimb.2025.1623154

COPYRIGHT

© 2025 Eidsaa, Sharma, Janasch, Kuch, Skoczyńska and Di Bartolomeo. This is an open-access article distributed under the terms of the Creative Commons Attribution Licens (CC BY). The use, distribution or reproduction in other forums is permitted, provided the original author(s) and the copyright owner(s) are credited and that the original publication in this journal is cited, in accordance with accepted academic practice. No use, distribution or reproduction is permitted which does not comply with these terms.

Proteomic landscape of imipenem resistance in Pseudomonas aeruginosa: a comparative investigation between clinical and control strains

Marius Eidsaa¹, Animesh Sharma^{2,3}, Markus Janasch¹, Alicja Kuch⁴, Anna Skoczyńska⁴ and Francesca Di Bartolomeo^{1*}

¹Department of Biotechnology and Nanomedicine, SINTEF Industry, Trondheim, Norway, ²Department of Clinical and Molecular Medicine, Norwegian University of Science and Technology (NTNU), Trondheim, Norway, ³Proteomics and Modomics Experimental Core (PROMEC) at NTNU and the Central Norway Regional Health Authority, Trondheim, Norway, ⁴Department of Epidemiology and Clinical Microbiology, National Medicines Institute (NMI), Warsaw, Poland

The increasing prevalence of antimicrobial resistance (AMR) poses a significant challenge to global health, particularly with bacterial pathogens such as Pseudomonas aeruginosa, a notorious cause of nosocomial infections. This study focuses on the comparative proteomic analysis of an imipenem-resistant strain of P. aeruginosa, a representative of world epidemic clone ST235, and a wildtype control strain, P. aeruginosa ATCC 27853, in response to varying concentrations of imipenem. Using label-free quantification (LFQ) and gene ontology (GO) enrichment analyses, we identified significant differences in the proteomic responses between the two strains. The clinical strain exhibited a stable proteomic profile across the imipenem gradient, suggesting preestablished and efficient resistance mechanisms that do not require extensive reconfiguration under antibiotic pressure. In contrast, the control strain showed a broader, more reactive proteomic response, particularly in proteins associated with membrane transport, stress response, and biofilm formation. Notably, uncharacterized proteins were significantly upregulated in the clinical strain, indicating potential novel resistance mechanisms. These findings highlight the distinct strategies employed by the two strains, with the clinical strain's stable resistance mechanisms contrasting sharply with the control strain's reactive approach. The study underscores the importance of further research into the uncharacterized proteins that may play crucial roles in antibiotic resistance, potentially leading to new therapeutic targets in the fight against AMR.

antimicrobial resistance, Pseudomonas aeruginosa, label-free quantitative proteomics, antibiotic challenge, imipenem

Highlights

 The clinical strain of *Pseudomonas aeruginosa* (ST235) showed a stable proteomic profile across imipenem concentrations, indicating established resistance mechanisms.

- The control strain (ATCC 27853) had a broader proteomic response, especially in membrane transport, stress response, and biofilm proteins.
- Upregulation of uncharacterized proteins in the clinical strain suggests possible new resistance mechanisms.

1 Introduction

Antimicrobial resistance (AMR) has emerged as a global health crisis, compromising the efficacy of traditional therapies against a diverse array of infections caused by bacteria, parasites, and fungi (Darby et al., 2023). This intricate biological phenomenon is primarily fueled by the selective pressure imposed by the widespread and often indiscriminate utilization of antimicrobials, which fosters an environment conducive to the survival and proliferation of resistant strains. The consequent outcome is an escalating prevalence of hard-to-treat infections (Fair and Tor, 2014).

Particularly alarming is the resistance demonstrated by bacterial pathogens. These organisms harness mechanisms such as horizontal gene transfer, mutation and selection, and adaptive resistance, to rapidly evolve and withstand antimicrobial agents (Davies and Davies, 2010). The rise of multi-drug resistant (MDR) and extensively drug-resistant (XDR) bacterial strains adds another layer of complexity to this scenario. These "superbugs" demonstrate resistance against multiple classes of antibiotics, posing serious therapeutic challenges and undermining patient outcomes (Magiorakos et al., 2012; Aslam et al., 2018).

Pseudomonas aeruginosa is an exemplar of such a resilient bacterial species. A notorious instigator of nosocomial infections worldwide, it demonstrates an exceptional ability to resist antibiotic therapies (Breidenstein et al., 2011; Langendonk et al., 2021). Given the robust resistance of such strains, treatment often resorts to lastline antibiotics, such as those in the carbapenem class. Imipenem, a member of this class, has a broader antimicrobial spectrum and higher potency than other beta-lactam antibiotics. It operates by interfering with bacterial cell wall synthesis, thus exerting a bactericidal effect. This antibiotic is often seen as a therapeutic beacon against a variety of MDR bacterial infections (Lautenbach et al., 2006; Xu et al., 2020). However, the growing overreliance on imipenem has inadvertently catalyzed the emergence of imipenemresistant P. aeruginosa strains, escalating the challenges associated with this formidable pathogen. A prime example of its adaptability is the clinical strain P. aeruginosa, recognized as a representative of world epidemic clone of sequence type ST235, owing to its extensive prevalence and heightened resistance to multiple antibiotics.

To effectively counter this rising tide of resistance, we must delve deeper into the molecular mechanisms underpinning the resistance of bacteria to potent antibiotics such as imipenem.

Proteomic analysis, in this regard, can prove instrumental by elucidating antibiotic resistance mechanisms at the protein level, as proteins are the ultimate executors of most cellular functions and interactions (Pérez-Llarena and Bou, 2016). Proteomics can offer invaluable insights into the adaptive responses of bacteria to antibiotic challenges. It achieves this by quantifying changes in protein expression, modifications, and interactions under different conditions. Proteome-wide label-free quantification, a technique frequently employed in proteomic analysis, allows for the comparison of protein abundance between resistant and susceptible strains, or between bacteria subjected to different antibiotic concentrations (Goodyear et al., 2023). As for this study, comparative proteomic studies serve as a potent investigative tool for understanding the profound and complex responses of bacteria to antibiotic exposure. They have an unprecedented ability to illuminate the molecular landscape where the dynamic interplay between antibiotics and bacteria unfolds. In the face of antibiotic stress, bacteria respond by expressing an array of proteins that enable them to neutralize the antibiotic's effect, remove the antibiotic from the bacterial cell, or modify the bacterial cell targets to evade the antibiotic's impact (Khodadadi et al., 2020). Proteomic studies, through their ability to quantitatively analyze the entire complement of proteins expressed under different conditions, enable us to delineate this intricate molecular proteomics pool in detail. The proteomic response of bacteria to antibiotics, which includes the alterations in protein expression, interactions, and modifications, is part of a larger adaptive response of bacteria to survive under antibiotic stress. This response forms the "resistome" of bacteria, a term coined to describe the collection of all the antibiotic resistance genes in a bacterial cell or community (Wright, 2007). While the concept of the resistome is predominantly genomic in nature, the functional output of the resistome is embodied in the proteome. It is the proteins, being the functional units of cells, that execute the instructions coded in the resistome, thereby manifesting the resistance phenotype (Sulaiman and Lam, 2022).

In the present study, we utilize the power of proteomics to dissect the resistome in action, as we analyze how two strains of P. aeruginosa - the representative of the world epidemic clone ST235 and the control strain ATCC 27853 - respond to the antibiotic imipenem, scrutinizing these profiles across a spectrum of escalating minimum inhibitory concentrations (MICs) of the antibiotic (Figure 1A). This nuanced approach will enable us to trace the dynamic shifts in protein expression and interactions as antibiotic pressure intensifies. Additionally, comparing the two selected strains will yield valuable insights into the proteomic signatures tied to the clinical strain's heightened resistance. Therefore, this research is primed to enrich our understanding of P. aeruginosa' s proteomic responses and the resistance mechanisms to imipenem. These insights may lead us towards potential solutions to the urgent and ongoing crisis of antimicrobial resistance by identifying proteins or pathways that could serve as novel targets for drug development or interventions that could disrupt the functionality of the resistome.

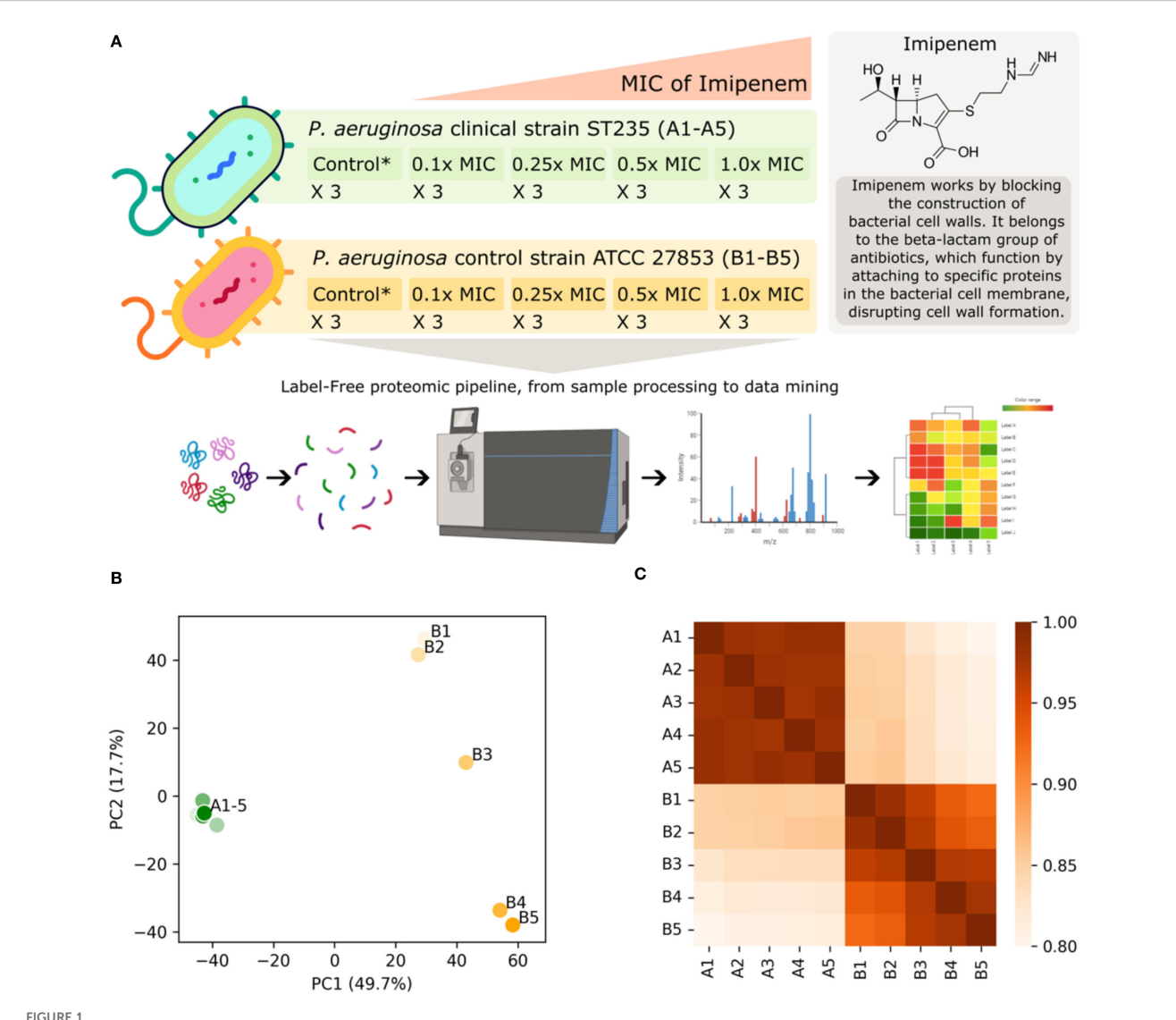


FIGURE 1
(A) This study involves a *P. aeruginosa* clinical strain (ST235) and a control strain (*P. aeruginosa* ATCC 27853), both subjected to increasing concentrations of imipenem based on their respective minimum inhibitory concentrations (MICs) with each condition replicated three times. Imipenem concentrations range from 1.6–16 mg/L and 0.2-2.0 mg/L for the clinical and control strains respectively, corresponding to 0.1x MIC, 0.25x MIC, 0.5x MIC and 1.0x MIC. The untreated control probes (no antibiotic) for each strain are indicated by Control* in the figure. The proteomic pipeline includes sample processing, mass spectrometry for label-free quantification, and data mining, leading to insights into differential protein expression and resistance mechanisms. Part of the figure has been created with BioRender.com (BioRender.com/w02t614). Below the graphical abstract, visualizations of the label-free quantification (LFQ) proteomics data sets are displayed, illustrating the impact of increasing imipenem concentration on the clinical (A1-5) and control (B1-5) strains: (B) Standard-scaled PCA plot shown for the two most significant principal components, accounting for 49.8% and 17.7% of the total variance. The imipenem-resistant clinical strain forms a compact cluster on the left-hand side, while the control strain exhibits a spread on the right-hand side. This spread shows a clear gradient from low antibiotic concentrations (lighter colors) at the top to high antibiotic concentrations (darker colors) at the bottom. (C) Heatmap of Spearman's correlation coefficients indicating a similar trend as observed in the PCA plot. It indicates a high overall correlation between the LFQ intensity scores, and particularly high correlations within the clinical strain.

2 Materials and methods

2.1 Strains

P. aeruginosa 6378/09 strain (NMI collection number), hereinafter referred to as clinical strain and *P. aeruginosa* ATCC 27853 control (reference) strain, obtained from American Type Culture Collection, were used for proteomic analysis. It is wildtype, imipenem-sensitive strain, hereinafter referred to as control strain.

The *P. aeruginosa* clinical strain was isolated from an oncology patient from an abdominal swab. It is an ESBL-negative, XDR strain, resistant to all important in therapy antibiotics (amikacin, aztreonam, cefepime, ceftazidime, ceftazidime/avibactam, ceftolozane/tazobactam, ciprofloxacin, colistin, imipenem, imipenem/relebactam, levofloxacin, meropenem, meropenem/vaborbactam, piperacillin/tazobactam, tobramycin) except colistin (MIC=2 mg/L). Resistance to imipenem is associated with VIM-2 variant of metallo-beta-lactamase (MBL), and the strain belonged to

world epidemic clone ST235, as previously described (Urbanowicz et al., 2021). ST235 has been the most frequent MDR/XDR *P. aeruginosa* clone globally, associated with VIM/IMP-like MBLs (Oliver et al., 2015) and VIM-2 are the most common variant of MBL globally (Mack et al., 2025).

2.2 Comparative analysis of the control and clinical strains genomes

The genomes of *P. aeruginosa* ATCC 27853 (Cao et al., 2017; BioProjectPRJNA377172, Accession number: CP011857) and NMI clinical strain ST235 (Urbanowicz et al., 2021; BioProject PRJNA701400, BioSample: SAMN17864755) were recruited from Genbank and compared using Bakta (ref: https://www.microbiologyresearch.org/content/journal/mgen/10.1099/mgen.0.000685), steps followed are available at https://github.com/animesh/pseudomonas_align_strains?tab=readme-ov-file#exact-commands-i-ran-for-bakta-in-this-project.

2.3 Determination of the minimum inhibitory concentration

Minimum inhibitory concentration (MIC) of imipenem (Merck KGaA, Darmstadt, Germany) was determined for both strains by the broth microdilution method according to standard ISO 20776-1 (ISO 20776-1, 2020). MIC (mg/L) ranges used in the tests were 1 – 512. The MIC was defined to be the lowest concentration at which no visible growth (complete inhibition of growth) of bacteria could be observed after incubation for 18 +/- 2 hours as recommended by the European Committee on Antimicrobial Susceptibility Testing (European Committee on Antimicrobial Susceptibility Testing, 2024).

2.4 Cell culture and antibiotic challenges

The bacteria were grown in cation-adjusted Mueller-Hinton broth (Becton Dickinson, Sparks, MD, USA) at 37°C with shaking (120 rpm) to optical density $OD_{600} = 1.0$. For antibiotic challenge, imipenem concentration of 0.1x MIC, 0.25x MIC, 0.5x MIC and 1x MIC of the particular strain was used in a volume of 5 ml. Bacterial cultures without the antibiotic were considered as untreated controls (see Figure 1A). Challenged bacterial cultures were then incubated with shaking (120 rpm) for 5 hours at 35°C +/- 2°C. Each experiment was performed three times for both clinical and control strains (3 biological replicates) with two technical replicates for each condition (antibiotic concentration). After incubation the bacterial cell pellets were harvested in pre-cooled Falcon tubes by centrifugation (5 min at 3,000 × g below 0°C). Then, the cell pellets were washed twice with ice-cold 1 x PBS (Sigma-Aldrich, Life Science, St. Louis, MO, USA). Finally, cell pellets were collected by centrifugation (5 min at 3,000 × g below 0°C), snap-frozen, and stored at -80°C until further testing (Liu et al., 2016; Hashemi et al., 2019; Jongers et al., 2021).

2.5 Label-free proteomics analyses

Proteins were quantified by processing the timsTOF-pro DDA MS-data using MaxQuant v2.0.3.0 (Tyanova et al., 2016). Namely, the following search parameters were used: enzyme specified as trypsin with a maximum of two missed cleavages allowed; minimum peptide length of 7; acetylation of protein N-terminal, oxidation of methionine, and deamidation of asparagine/glutamine as dynamic post-translational modification. These were imported in MaxQuant which uses m/z and retention time (RT) values to align each run against each other sample with a minute window matchbetween-run function and 20 mins overall sliding window using a clustering-based technique. These were further queried against the reference-proteome of P. aeruginosa downloaded from UniProt (UniProt Consortium, 2022) in May 2022 and MaxQuant's internal contaminants database using Andromeda built into MaxQuant. Both Protein and peptide identifications false discovery rate (FDR) was set to 1%, only unique peptides with high confidence were used for final protein group identification. Peak abundances were extracted by integrating the area under the peak curve. Each protein group abundance was normalized by the total abundance of all identified peptides for each run and protein by calculated median summing all unique peptide-ion abundances for each protein using label-free quantification (LFQ) algorithm (Cox et al., 2014) with minimum unique peptide(s) \geq 1. The mass spectrometry proteomics data have been deposited to the ProteomeXchange Consortium via the PRIDE (Perez-Riverol et al., 2022) partner repository with the dataset identifier PXD055744 (Username: reviewer_pxd055744@ebi.ac.uk Password: XNtCwVbI4AIs).

2.6 Data processing and mining

Having obtained the label-free quantification (LFQ) intensity values for both the P. aeruginosa clinical strain and control strain, across the five different concentrations (as depicted in Figure 1A), we performed a series of data filtering, processing, and aggregation steps, including removal of reverse hits and potential contaminants to ensure the integrity of our data. In the case of multiple UniProt protein IDs per hits, the one with the highest curation status were used in the downstream analysis when relevant. This led to a total of N=3811 proteins in our analysis, accounting for approximately 60% of the chromosomal genes in an average P. aeruginosa strain (Mosquera-Rendón et al., 2016).

For each strain and antibiotic concentration, we had three biological replicates (Figure 1A). We performed a standard t-test using the log2-transformed LFQ (log2LFQ) values for each protein ID to obtain the associated p-values. These p-values were then corrected using the Benjamini-Hochberg False Discovery Rate

(FDR) procedure. This was done for all experiments with non-zero MIC, using the 0.0x MIC as a control for each strain. This means that we compared LFQ values and performed *t*-tests within strains only. Alongside the *t*-test, *p*-value and the FDR values, we used the median value for LFQ intensities where applicable.

When comparing LFQ intensity values between experiments, we primarily used fold change relative to the control probe (no antibiotic) to describe the difference in log2 space, expressed via log2LFQ values. Proteins with LFQ intensity values of zero for both the control probe (no antibiotic) and 1.0x MIC experiments were excluded. Proteins with values of zero in one experiment and nonzero in another were assigned a large, finite fold-change value. When comparing across strains, we used the median log2LFQ fold changes between the strains, as these values were already normalized with respect to the 0.0x MIC control experiment for the respective strains.

Unless otherwise specified, the intra-strain protein LFQ intensity fold-change cutoff was set at 1.5, or approximately ± 1.5 0.5849 after log2 transformation. In the individual protein volcano plots an uncorrected p-value cutoff of 0.1 was employed, with values above colored grey and values below colored light red or blue, while FDR values below 0.1 are furthermore indicated by dark red or blue color. These thresholds are not particularly conservative, which is deemed appropriate given the explorative nature of the study. The individual protein volcano plot x-axis and y-axis ranges were fixed to improve visual comparability, and log2 fold changes were visually capped at ± 1.5 1 alongside ± 1.5 2 alongside ± 1.5 3 alongside ± 1.5 5 along

To visualize the overall features of the data set, we calculated and used a Principal Component Analysis (PCA), using standard scaling, and a correlation matrix (heatmap) of Spearman's correlation coefficients between experiments. This provided an overview of the structure and relationships in the data set (Figures 1B, C).

2.7 Gene-ontology enrichment analysis

To discern significant systemic alterations in the proteomes within and across strains and antibiotic concentrations, we conducted a Gene Ontology (GO) term enrichment analysis. This method is set-based, meaning that groups of proteins are compared rather than individual proteins. Statistical tests are performed by comparing a subset to the full background set. The GO term enrichment analysis aims at finding enriched functional, process-related, and compartmental annotations associated with each protein in the subset. Collectively, numerous individually insignificant protein-level changes can be linked to statistically significant features on aggregate, cellular level.

The GO term enrichment analysis is agnostic to the subset selection method. Therefore, we employ both FDR-value, uncorrected *p*-values, and no *p*-value thresholds when selecting proteins, in conjunction with fold-change thresholds, at various parts of the analysis. We performed statistical tests based on hypergeometric distributions on the subset selection, and subsequently corrected these using the Benjamini-Hochberg FDR

procedure, setting the FDR-value threshold to 0.1. Both over-representation and under-representation were accounted for in the analyses. The choice of background, i.e., the full set against which the subset is compared, is crucial for obtaining accurate results. For this, we used all mapped and processed proteins with well-defined *t*-tests based on the three biological replicates.

We collected GO term information for *P. aeruginosa* using UniProt, release: 2024_03 (UniProt Consortium, 2023), and mapped the GO term IDs onto the Gene Ontology Knowledgebase using AmiGO 2, version: 2.5.17 (Ashburner et al., 2000), aligning the information with the UniProt IDs. Out of 3811 proteins, 3253 were associated with GO terms, and the remaining were assigned a placeholder value to ensure their inclusion in the analyses, since the non-annotated proteins may be of particular interest for further study.

In the results, we visualized the enriched GO terms using volcano plots. The x-coordinate of each GO term represents the log2 value of its enrichment (blue indicates under-representation and red indicates over-representation), and the range is fixed and visually capped at +/- 2.5. The y-coordinate represents the FDR values associated with each GO term (not to be confused with the protein-level FDR-values). The area of the GO-term circles is proportional to the number of proteins associated with the GO term in the subset. All terms with a GO-term FDR value > 0.1 are indicated in grey and are excluded from further analysis.

2.8 Resources and tools

Data analyses and visualizations were performed using Python 3.11, along with standard modules such as numpy, pandas, scipy, matplotlib, and seaborn, among others. The t-tests and dose-correlation statistics were conducted using R.

3 Results

Here, we present the results of our comparative proteomic investigation between the P. aeruginosa world epidemic clinical strain and the wildtype control strain under four increasing concentrations (in mg/L): 1.6, 4, 8, 16 and 0.2, 0.5, 1.0, 2.0, which equates to 0.1x, 0.25x, 0.5x, and 1.0x MIC for the clinical and control strains respectively. The proteome data, acquired and processed as described in the Materials and Methods section, comprised a total of N=3811 proteins. For each protein, we calculated the LFQ intensity values across the five concentrations for both strains. Subsequently, a t-test was performed across the biological replicates, using the control probe (no antibiotic) experiments as controls, to derive protein-specific p-values.

3.1 Results overview

Comparative genomes analysis revealed that both strains demonstrate a significant degree of similarity, with nearly 4,000

potential gene products shared between them. The fundamental functions of Pseudomonas aeruginosa remain preserved. Notwithstanding the phylogenetic divergence, there exists considerable overlap alongside a common pool of potential target proteins. However, the control strain lacks the distinctive set of resistance factors present in ST235, which confer a strategic advantage in clinical settings (Supplementary Figure S2) along with 573 and 835 hypothetical protein in ATCC 27853 and ST235 respectively (Supplementary Table T2).

Exploration of the overall trends in the data, as visualized in Figures 1B, C, suggests that the protein abundance in the clinical strain remains stable under the influence of imipenem, unlike the control strain. The PCA plot (Figure 1B) reveals that the largest variance between the experiments is attributed to the strains themselves (PC1, x-axis). The second largest factor of variance (PC2, y-axis) corresponds to the increasing imipenem concentration, as evidenced by the gradual transition from control probe (no antibiotic) in the top-right to 1.0x MIC in the bottom-right for the control strain. The heatmap (Figure 1C) displays a highly intercorrelated block in the top-left corner, representing the clinical strain experiments. The bottom-right corner shows a slight but clear gradient towards covariance among experiments with similar imipenem concentrations. Notably, there is high similarity between the strains, with correlation coefficients around 0.85 for the control probes (A1 and B1) and 0.80 at 1.0x MIC (A5 and B5).

3.2 Proteomic changes within strains

Based on the overall results from Figures 1B, C, we expect the significant fold changes for individual proteins across MIC concentrations to be more pronounced for the control strain than the clinical strain. The volcano plots in Figure 2 confirms this prospect. Here, we have plotted the N=3811 proteins with a fold change threshold of 1.5 for both the control (Figure 2A) and clinical (Figure 2B) strains at 1.0x MIC, as compared with a t-test to 0.0x MIC (see Materials and Methods for details).

In these plots, an increase in fold change from 0.0x MIC to 1.0x MIC, i.e. up-regulation, is depicted by red dots, while a decrease in fold change, i.e. down-regulation, is represented by blue dots. Each dot corresponds to a protein. For both strains, we display the proteins with *p*-values above 0.1, and fold change below the threshold, as grey, while light red and blue denote *p*-values below 0.1 and full (darker) red and blue depict the proteins with FDR corrected *p*-values below 0.1. As expected, the control strain shows a range of significant FDR values, while the clinical strain only has 8 proteins fulfilling the criteria: AmpC (P24735), PA0868 (Q91573), DDAH (Q914E3), Tse4 (Q91069), PA2547 (Q910T7), PA0207 (Q916T1), VreR (G3XCU5) and PhzB2 (Q9S508). These proteins (depicted in the top corners of Figure 2B) are further explored in Figure 3 and Supplementary Table S1 and detailed results will be presented in the following subsection.

For the normalized 1.0x MIC control strain experiments, displayed in Figure 2A, there are n=601 proteins with FDR value

below 0.1 which show a fold change greater than 1.5 (depicted in dark red and blue), and n=1219 proteins adhere to the fold change threshold alone. The respective numbers for the clinical strain are n=8 (where n=79 have an uncorrected p-value below 0.1) and n=358, as visualized in Figure 2B.

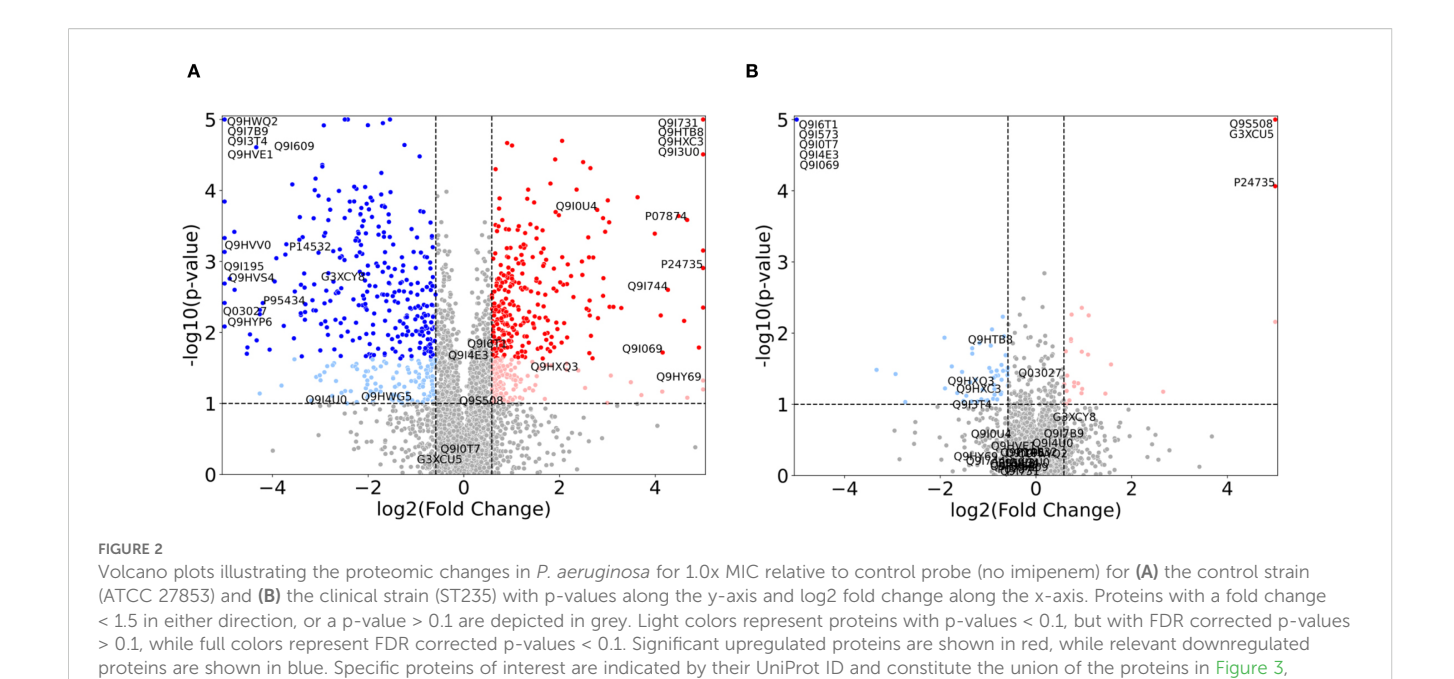
3.3 Comparison of specific proteins

As mentioned in the previous section, 8 proteins passed the FDR value threshold of 0.1 for the clinical strain, making them resistome candidates which are significantly involved in the antimicrobial resistance in P. aeruginosa. These proteins are shown in Figure 3, where Figures 3A-D show an overall downregulation of the specific protein in the clinical strain (in green) for increasing MIC, Figures 3E-F show an overall up-regulation for increasing MIC, while Figures 3G-H show a particularly large difference between the strains, i.e., where the LFQ intensity in the clinical strain is much lower than the control strain. The control strain (in orange) shows an overall trend towards up-regulation for these 8 proteins, aside from the proteins in Figures 3C, D. The standard deviations, indicated by shaded green for the clinical strain and shaded orange for the control, vary. Large standard deviations, such as for PA0868 (Q9I573) in Figure 3D, indicate high variability in protein expression, while the high-LFQ intensity protein AmpC (P24735) in Figure 3F displays a clear signal, suggesting consistent protein expression across replicates. The dose-correlation statistics were calculated for all proteins for both strains, but since the number of measurements per protein is low, the associated pvalues are poor, potentially making the correlation values misleading. Consequently, the specific dose correlation values will not be discussed here, but please refer to Supplementary Tables S3 and S4 for details on clinical and control strains respectively.

The proteins in Figure 3 are described in more detail in Supplementary Table S1, where a description and associated gene ontologies are added (see Materials and Methods for details). These findings and their implications for understanding antimicrobial resistance in *P. aeruginosa* will be discussed further in the Discussion section.

3.4 GO term enrichment within strains

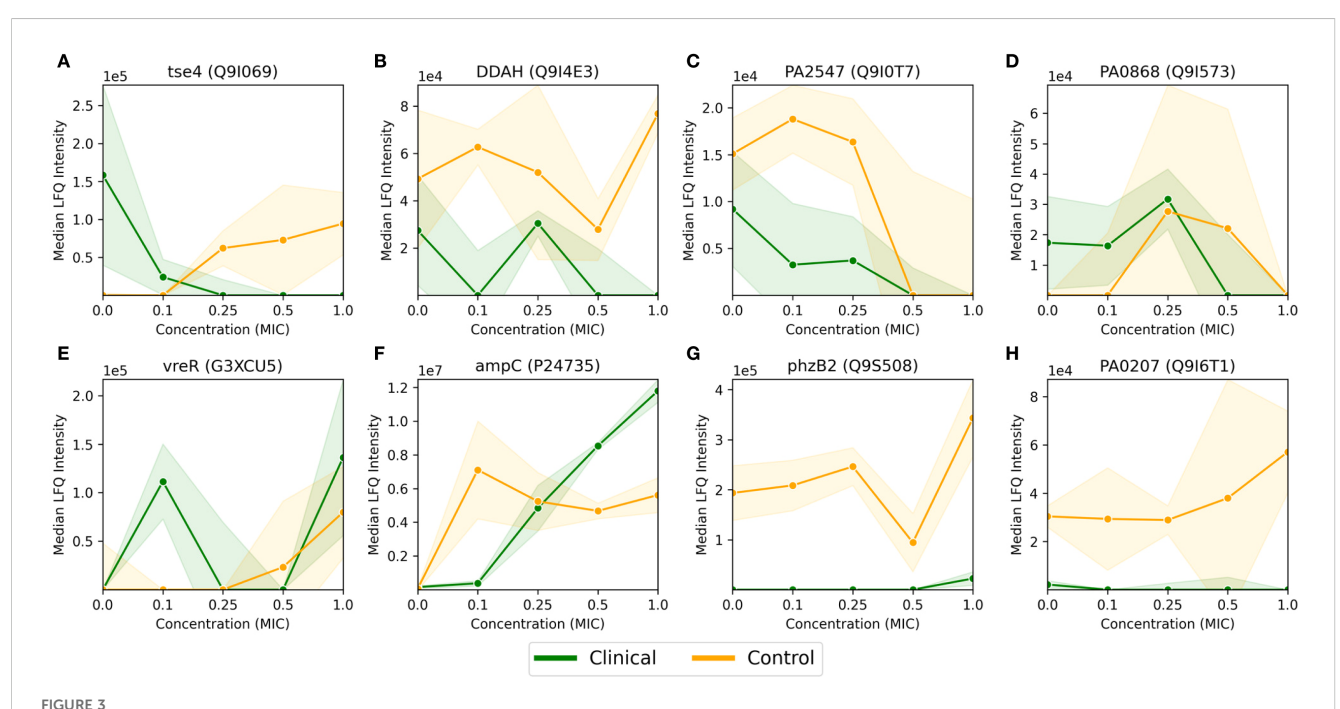
To better understand the biological implications of the significant up- and downregulated protein subsets (highlighted in red and blue in Figure 2), we conducted a GO term enrichment analysis as outlined in the Materials and Methods section. This analysis allows us to assess the biological relevance of our protein subsets, indicated by the enrichment of biological traits, when compared to the original full set of N=3811 proteins. By comparing high-fold-change proteins between 1.0x MIC and control probe (no imipenem), we can identify the biological functions and processes that the organism upregulates or downregulates. This comparison also provides p-values, which can furthermore be FDR corrected, indicating the statistical



significance of these enrichments. I.e., there are two levels of (corrected) *p*-values at this stage: (i) protein-level *p*-values, based on *t*-tests for individual proteins, as depicted in Figure 2, and (ii) protein-subset level *p*-values, where enrichments of protein annotations in the subset compared to the full, original set are assessed via hypergeometric processes. Thus, a random selection of proteins, which does not reflect real biology, is expected to meet the

Supplementary Figure S1 (and Supplementary Tables S1, S2).

protein-subset level, GO-term FDR threshold of 0.1, thus reducing the overall likelihood of false positive GO-term enrichment scores at 10%. In the following, we present results based on the union of upregulated (red) and downregulated (blue) proteins, as depicted in Figure 2. GO term analysis was performed on up- and downregulated proteins separately, but these results were too similar to the union set, when combined, to warrant a separate



Median LFQ intensity scores plotted against increasing fractions of MIC, ranging from no antibiotic (zero concentration) to 1.0x MIC, for 8 proteins (A-H) passing the FDR corrected t-test for the *P. aeruginosa* clinical strain, as displayed in Figure 2B. The clinical strain is shown in green, the control strain is shown in orange, and the shaded area depicts the associated standard deviations (n=3) among the replicates with a linear interpolation between the measurements.

discussion. The GO term enrichment analyses were conducted for both the control and clinical strains of *P. aeruginosa* (Supplementary Figure S1).

Table 1A provides a list of the significantly enriched GO terms (Supplementary Figure S1A) with their respective statistics. Noteworthy terms include proteins associated with various cellular components (e.g., periplasmic space, cytosol, cytoplasm, and membrane), transporter activities (peptide transmembrane, efflux transmembrane, ABC-type sulfate and siderophore), DNA interactions, and specific processes (e.g., pyoverdine biosynthesis and iron ion transport). The clinical strain where only the fold-change threshold is applied, displayed in Table 1B (Supplementary Figure S1D), exhibits some of the same terms as in Table 1A, albeit with lesser significance overall. A unique feature here is the enrichment of proteins without associated GO term annotations, which, with an enrichment score of 1.52, is still significant due to the substantial number of proteins in the "NOGO" pseudo-term as GO annotations are missing.

3.5 Differential protein expression and GO term enrichment

To understand the proteomic landscape of imipenem resistance in *P. aeruginosa*, we have thus far delved into within-strain comparisons, specifically between the 1.0x MIC and control probe (no antibiotic) experiments. We have also cross-compared these results between the clinical and control strains. Now, we consider a more direct comparison across strains, by using the difference between the normalized, log2-transformed LFQ values of the control and clinical strains as a measure of fold-change (see Materials and Methods for details).

The volcano plots depicted in Figures 4A, C illustrate fold-change thresholds of 1.5 and 8 respectively (equivalent to approximately +/- 0.585 and exactly +/- 3 in log2 space respectively). The reason for these choices stems from Figure 2, where we wanted a comparable example (Figure 4A) as well as a suitably sparse counter example, where only proteins with large differences in expression are included (Figure 4C). Other thresholds could be chosen, but we found a >8-fold change threshold to be a good compromise between sparsity and representativeness. The FDR corrected p-values displayed on the y-axis are derived from the control strain t-test. These are included for visual comparability with Figure 2 and are not considered in the GO term enrichment analysis displayed in Figures 4B, C.

As Figures 1B, C demonstrate, the clinical strain's overall protein expression is not significantly affected by increasing MIC. Consequently, we anticipate that the normalized differential protein expression will mirror the results observed in the control strain. This expectation is confirmed in Figure 4B (and Supplementary Figure S1C). A noteworthy change, however, is the enrichment of proteins associated with magnesium ion binding.

A GO term enrichment analysis was conducted using the 146 proteins with fold change of more than 8, denoted by blue and red dots in Figure 4C. The results of this analysis are presented in

Figure 4C and further detailed in Table 1C. The proteins involved are provided in Supplementary Table S8 (in the "IDs" column).

Several of these terms are recognizable from protein subsets seen in e.g. Table 1A, but there are also differences from earlier protein subsets. These include transport terms like glycine betaine, amino-acid betaine, and carnitine transmembrane transport. There are specific enzyme-related terms such as sigma factor antagonist and cytochrome-c peroxidase, along with chaperone-mediated protein complex assembly. The list also includes cellular responses to hyperosmotic salinity and sulfur starvation, protein secretion by the type III secretion system, alginic acid biosynthesis, and structures like the extracellular region and host cell membrane. It is also important to highlight the n=33 proteins not associated with any known GO terms, representing a significant overrepresentation. These proteins, along with other specific proteins, will be the focus of our investigation in the subsequent section.

3.6 Comparison of selected proteins with large differential protein expression between strains

In Figure 4, we visualized the differential protein expression comparing the difference in the clinical strain to that of the control strain, and in Figure 4C, we applied a threshold demanding this difference to be >8-fold. Here, we will delve into some of the proteins adhering to this threshold. To obtain a manageable number of proteins, we employed some criteria for selection: (i) low or negative correlation values (< 0.4) between clinical and control strain across the control probe (no antibiotic) plus 4 imipenem concentrations (0.1x, 0.25x, 0.5x and 1.0x MIC), (ii) striking differences in expression, and/or (iii) part of significantly enriched GO terms in Table 1C. This process led us to 26 proteins, 24 of which are shown in Figure 5. The remaining two proteins are Tse4 (Q9I069), already displayed in Figure 3A, and PpiC2 (Q9HWK5) which is highly expressed in the clinical strain, and comparably non-expressed in the control across all concentrations. The remaining 24 proteins are split so that Figures 5A-O has an overall downregulation for the control for increasing imipenem concentrations, while Figures 5P-X show an overall up-regulation for the control. The clinical strain displays more stability across varying concentrations, which is not surprising given the results shown in Figures 1B, C. However, Figures 5S, W, alongside Figure 3A, displaying the proteins Wzm (Q9HTB8), PA0101 (Q9I731) and Tse4 (Q9I069) respectively, also show clear downregulation in the clinical strain for increasing concentrations, in addition to the up-regulation in the control strain. As in Figure 3, the standard deviations are shown as green (clinical) and orange (control) shading, where linear interpolation has been used between the measurements. While several proteins display large standard deviations for the clinical strain, most control strain trends are associated with comparably small standard deviations. This indicates a clear biological effect of increasing concentrations of imipenem for the P. aeruginosa (ATCC 27853) control strain which can be related to these proteins and their associated functions and

TABLE 1 Enriched GO terms, color coding: light red for over-represented (enriched) and light blue for under-represented ("under-enriched") terms.

Label	GO ID	Enrichment	Size	FDR	GO term					
(A) Control str	(A) Control strain for protein <i>t</i> -test FDR < 0.1 and fold change > 1.5 (label from Supplementary Figure S1A)									
A	GO:0042597	3.158	38	1.39e-09	periplasmic space					
В	GO:0005829	0.431	35	3.57e-08	cytosol					
ОС	GO:0030288	3.143	23	2.12e-05	outer membrane-bounded periplasmic space					
D	GO:0003700	0.296	10	6.55e-05	DNA-binding transcription factor activity					
E	GO:0003677	0.306	9	3.37e-04	DNA binding					
F	GO:0005737	0.557	41	3.37e-04	cytoplasm					
G	GO:1904680	5.381	7	3.82e-03	peptide transmembrane transporter activity					
Н	GO:0002049	3.758	11	3.82e-03	pyoverdine biosynthetic process					
I	GO:0043190	2.54	19	6.25e-03	ATP-binding cassette (ABC) transporter complex					
O J	GO:0006355	0.441	15	7.81e-03	regulation of DNA-templated transcription					
K	GO:0038023	3.417	10	0.0189	signaling receptor activity					
L	GO:0015562	3.075	11	0.0258	efflux transmembrane transporter activity					
M	GO:0006826	3.913	7	0.0483	iron ion transport					
N	GO:0042938	5.125	5	0.0483	dipeptide transport					
O O	GO:0015419	6.15	4	0.0518	ABC-type sulfate transporter activity					
P	GO:0005886	1.325	100	0.0568	plasma membrane					
Q	GO:0015891	4.1	6	0.0594	siderophore transport					
R	GO:0005615	3.28	8	0.0594	extracellular space					
S	GO:0016020	1.394	68	0.0856	membrane					
Т	GO:0033103	3.69	6	0.0982	protein secretion by the type VI secretion system					
U	GO:1990281	3.311	7	0.0982	efflux pump complex					
(B) Clinical strain with fold change > 1.5 (label from Supplementary Figure S1D)										
A	GO:0005737	0.386	17	1.51e-04	cytoplasm					
В	GO:0005524	0.336	12	1.56e-04	ATP binding					
С	GO:0042597	3.131	21	4.65e-04	periplasmic space					
D	GO:0005829	0.493	24	1.73e-03	cytosol					
Е	NOGO	1.52	77	9.55e-03	No known GO terms					
(C) Differential	(C) Differential protein expression (label from Figure 5D)									
A	GO:0042597	6.158	18	4.02e-08	periplasmic space					
В	GO:0005829	0.152	3	1.92e-04	cytosol					
C	GO:0031460	10.126	4	0.0155	glycine betaine transport					
D	GO:0016989	10.126	4	0.0155	sigma factor antagonist activity					
Е	GO:0043190	4.403	8	0.0155	ATP-binding cassette (ABC) transporter complex					
F	GO:0042121	8.438	5	0.0155	alginic acid biosynthetic process					

(Continued)

TABLE 1 Continued

Label	GO ID	Enrichment	Size	FDR	GO term				
(C) Differential protein expression (label from Figure 5D)									
G	GO:0071475	12.658	3	0.0263	cellular hyperosmotic salinity response				
Н	GO:0015838	12.658	3	0.0263	amino-acid betaine transport				
I	GO:0015226	12.658	3	0.0263	carnitine transmembrane transporter activity				
O J	GO:1902495	25.315	2	0.0295	transmembrane transporter complex				
K	GO:0010438	25.315	2	0.0295	cellular response to sulfur starvation				
L	GO:0005576	4.467	6	0.0319	extracellular region				
M	NOGO	1.622	33	0.0405	No known GO terms				
N	GO:0030254	6.329	4	0.0429	protein secretion by the type III secretion system				
0	GO:0051131	16.877	2	0.0574	chaperone-mediated protein complex assembly				
P	GO:0015418	16.877	2	0.0574	ABC-type quaternary ammonium compound transporting activity				
Q Q	GO:0004130	12.658	2	0.0986	cytochrome-c peroxidase activity				
R	GO:0033644	12.658	2	0.0986	host cell membrane				

compartments. More information about the proteins in Figure 5 can be found in Supplementary Table S2, including their UniProt description (UniProt Consortium, 2023) and associated GO terms (Ashburner et al., 2000). Some proteins, PA2384 (Q9I195), PA4129 (Q9HWQ2), PA1469 (Q9HVV0), PA1034 (Q9I4U0), PA1404 (Q9I3U0) and PA0101 (Q9I731), in Figures 5C, D, I, M, P, W respectively, are uncharacterized and have thus no associated GO terms. An additional observation to remark in Figure 5 is the high relative expression of certain proteins in the clinical strain at 0 MIC (control probe), as well as the quasi-absence of other proteins, both groups largely displaying also the aforementioned stability over the different antibiotic concentrations. Both groups, constitutively high expressed or absent proteins in the clinical strain, belong largely to transporter protein and outer membrane and cell wall GO terms. These results will be further analyzed in the Discussion section, where we will shed light on their potential association with imipenem and antimicrobial activity.

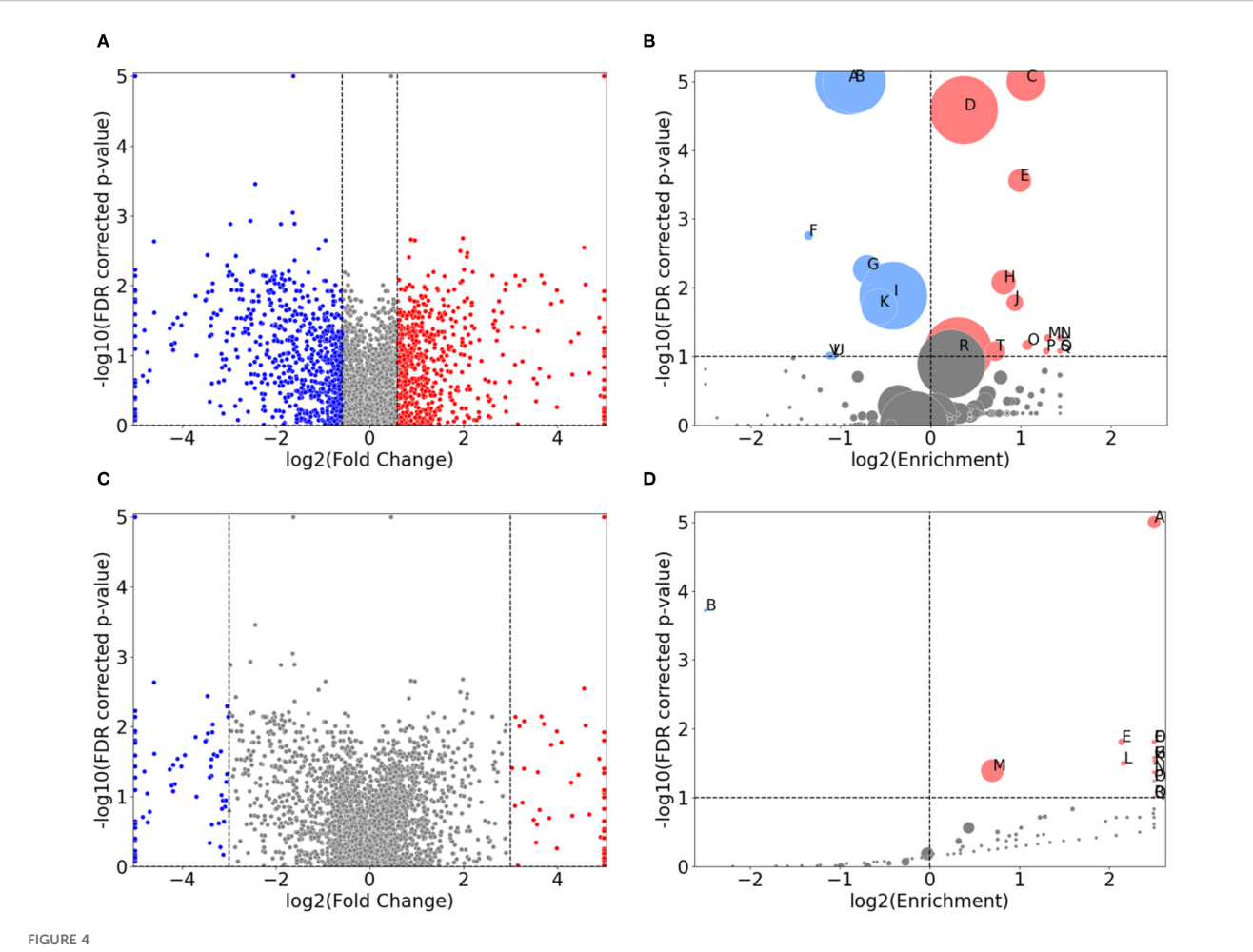
4 Discussion

The proteomic landscape of *P. aeruginosa* under the influence of imipenem, a commonly used carbapenem antibiotic, has been the subject of investigation in this study revealing key insights into the molecular mechanisms of antimicrobial resistance. Our comparative analysis between the world epidemic clinical strain and the control strain has highlighted changes in the proteome that occur in response to varying imipenem concentrations. Utilizing normalized label-free quantification (LFQ) intensities, protein group level *t*-tests, and Gene Ontology (GO) enrichment analysis of protein subsets, we have been able to delve deeper into the molecular mechanisms of imipenem resistance.

The observed differences in minimum inhibitory concentrations (MICs) between the clinical and control strains (Figure 1) underscore the clinical strain's enhanced resistance to imipenem, reflecting its ability to survive under antibiotic pressures that typically inhibit or kill susceptible strains (Leigue et al., 2016). The varying antibiotic concentrations provide a suitable framework to explore the adaptive proteomic responses of both strains, revealing molecular adaptations associated with resistance.

In the clinical strain, eight proteins are identified as significant, displayed in Figure 3, each playing a role in the resistance strategy and with wide-reaching implications for understanding the mechanisms of imipenem resistance in P. aeruginosa. The upregulation of beta-lactamase (AmpC, P24735) is consistent with its well-documented role in hydrolyzing beta-lactam antibiotics, including imipenem, and it is known to belong in a group of enzymes that provide multi-resistance to antibiotics (Jacoby, 2009). Its overexpression in the clinical strain could be a direct response to the antibiotic pressure, leading to the degradation of imipenem and thus, resistance (Berrazeg et al., 2015; Barbier et al., 2023; Elfadadny et al., 2024). In addition, also the sigma factor regulator VreR (G3XCU5), another upregulated protein, is likely involved in modulating the expression of genes that help the strain withstand antibiotic-induced stress, contributing to its resilience (Matilla et al., 2022).

Interestingly, Tse4 (Q9I069), a toxin protein associated with the Type VI secretion system, is downregulated in the clinical strain. This could potentially be caused by protein degradation. While RNA-seq data is not available for this study, future investigations comparing mRNA levels with protein expression could provide further insights. However, this could suggest a strategic conservation of resources, where the strain prioritizes essential survival functions over energy-intensive processes like toxin

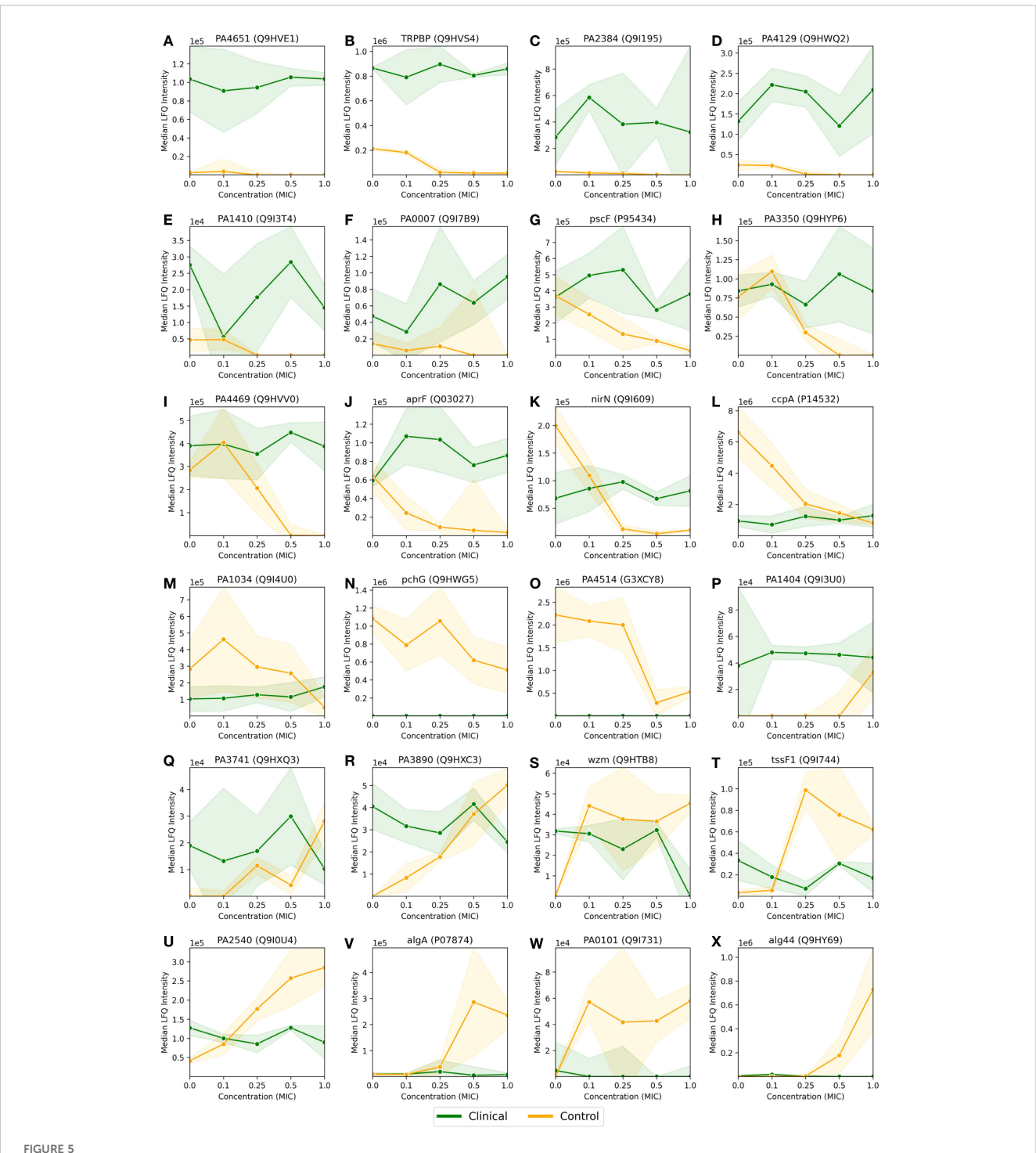


Direct comparison of protein expression between the control-probe-normalized control strain and clinical strain for 1.0x MIC imipenem treatment. (A, C) are volcano plots displaying the normalized differential protein intensity fold-change along the x-axis, with a fold-change threshold of 1.5 and 8, respectively. Red dots have larger positive fold change in the control strain, from 1.0x MIC relative to control probe (no antibiotic), compared to the clinical strain, and, correspondingly, larger negative fold change for the blue dots. (B, D) are GO term volcano plots for the protein subset based on the non-grey proteins in (A, B) respectively. The FDR values along the y-axis in (A, C) are derived from the control strain and applied for visual comparison.

production under antibiotic stress. The associated GO terms, such as "beta-lactamase activity" (GO:0008800) and "sigma factor antagonist activity" (GO:0016989), highlight the biochemical pathways enhanced in response to imipenem, pointing to a multifaceted resistance mechanism involving both direct antibiotic degradation and stress response modulation. In contrast, the control strain exhibits a broad activation of cellular pathways in response to increasing imipenem concentrations.

Based on the Gene Ontology (GO) terms enriched in the *P. aeruginosa* control strain comparing 1.0x MIC to the (no imipenem) control probes, as outlined in Table 1A, there are several key processes of interest. The significant enrichment of GO terms related to membrane integrity and transport processes, such as "periplasmic space" (GO:0042597) and "efflux transmembrane transporter activity" (GO:0015562), suggests a defensive strategy focused on expelling the antibiotic and maintaining membrane stability (Young et al., 2019; Heywood and Lamont, 2020).

The upregulation of proteins involved in the "pyoverdine biosynthetic process" (GO:0002049) further indicates an enhancement of iron acquisition systems, potentially as a countermeasure to the oxidative stress imposed by imipenem. In addition, the production of pyoverdines, siderophores is essential for iron acquisition, growth and survival by mediating biofilm formation and pathogenicity (Dell'Anno et al., 2022). In addition to the broader activation of intracellular processes, as indicated by the enrichment of GO terms like "cytosol" (GO:0005829) and "cytoplasm" (GO:0005737), there is significant enrichment of terms related to the "ATP-Binding Cassette (ABC) Transporter Complex", which may play a role as an antibiotic efflux transporter (Lewis et al., 2012). Also noteworthy is the involvement of Type VI Protein Secretion System Complex, often linked to biofilm production as an antagonistic mechanism (Hespanhol et al., 2023). Interestingly, some studies suggest that imipenem can inhibit biofilm production, which is associated with Type VI Secretion System (de Sousa et al., 2023). This further illustrates



Median LFQ intensity scores plotted against increasing fractions of the MIC, ranging from no imipenem (zero concentration) to 1.0x MIC, for 24 proteins (A-X) with particularly large and/or interesting differential protein expressions between the *P. aeruginosa* clinical and control strains, as displayed by red and blue dots in Figure 4C. The clinical strain is shown in green, the control strain is shown in orange, and the shaded area depicts the associated standard deviations (n=3) among the replicates with a linear interpolation between the measurements.

the control strain's strategy to activate a broad spectrum of defensive pathways to cope with antibiotic threat.

As reflected by the results from Supplementary Figure S1D and Table 1B, the proteomic response in the clinical strain is more targeted, it involves fewer GO terms, reflecting stable resistance mechanism that does not require extensive proteasomal

reconfigurations. The enrichment of "periplasmic space" (GO:0042597) and "cytosol" (GO:0005829) suggests that the clinical strain, like the control strain, emphasizes membrane integrity and cytoplasmic processes. However, the clinical strain does not show a broad spectrum of activated pathways, suggesting either pre-existing or well-adapted mechanisms that require little

alteration in response to imipenem. The relatively high expression of certain proteins at 0x MIC and their invariance across the different imipenem concentrations, as well as the absence of other proteins over the entire concentration range displayed in Figure 5 can be interpreted as a result of evolutionary adaptations of the genome of clinical strain (Treepong et al., 2018). Long-term exposure to antibiotic can change the expression regulation of genes causing constitutive presence or absence of genes, in this case largely belonging to outer membrane, cell wall and transporter GO terms, if not yet uncharacterized. What is remarkable, is the significant enrichment of uncharacterized proteins, indicated by the "NOGO" term, suggesting that the clinical strain may use novel or less-characterized proteins to its resistance strategy, e.g. by proteins like PA2384 (Q9I195) or PA4129 (Q9HWQ2) in Figures 5C, D, to be further discussed below. This is indicative of potential areas where further research could uncover new aspects of antimicrobial resistance. If confirmed, and further investigated, the role of these proteins might underscore novel proteomic profiles linked to adaptation to antibiotic stress.

A direct comparison of protein expression between the clinical and control strains at 1.0x MIC reveal a clear difference in their strategies to cope with imipenem (Figure 4D; Table 1C). The control strain shows substantial upregulation of proteins involved in membrane and transport processes, reflecting a reactive and broadspectrum response to antibiotic pressure. The significant enrichment of GO terms like "glycine betaine transport" (GO:0031460) and "ABC transporter complex" (GO:0043190) suggests that the control strain activates mechanisms to manage osmotic stress and expel imipenem, respectively. Glycine betaine is known to protect cells against osmotic stress (Zhao et al., 2018), and its increased transport activity could be part of the control strain's attempt to mitigate the effects of imipeneminduced stress. In contrast, the clinical strain shows enrichment in oxidative stress management pathways, such as "cytochrome-c peroxidase activity" (GO:0004130), highlighting its focus on specific oxidative stress management rather than broad reactive changes. The presence of "extracellular region" (GO:0005576) enrichment in the clinical strain suggests it may involve extracellular defense mechanisms, potentially modifying or interacting with its environment to resist the antibiotic. The pronounced differences in protein expression and overall cellular responses to imipenem between the clinical and control strains of P. aeruginosa are further elucidated by the analysis of selected proteins with >8-fold differential expression, as visualized in Figure 5. The clinical strain's ability to maintain a relatively stable proteomic profile across varying concentrations of imipenem contrasts starkly with the control strain's more reactive and fluctuating proteomic responses, which likely reflect a broad-spectrum attempt to mitigate antibiotic stress. Uncharacterized proteins, such as PA2384 (Q9I195) and PA4129 (Q9HWQ2), exhibit significant upregulation in the clinical strain, suggesting these proteins may be integral to its resistance mechanisms. The consistent expression of these proteins, even under high antibiotic pressure, indicates a potentially critical role in the clinical strain's adaptation and survival. This upregulation, coupled with the stable expression of well-characterized proteins like AprF (Q03027) and AlgA (P07874), underscores the clinical strain's reliance on pre-established resistance

mechanisms, which seem to operate efficiently without the need for extensive proteomic reconfiguration in response to imipenem. In contrast, the control strain demonstrates significant proteomic shifts, particularly in proteins associated with membrane transport and stress response, such as PA4514 (G3XCY8) and Wzm (Q9HTB8). These shifts reflect the strain's reactive adjustments to counteract the effects of imipenem, emphasizing a less specialized and more variable approach to resistance. The marked increase in expression of alginate biosynthesis proteins in the control strain at higher MICs also suggests an attempt to enhance biofilm formation as a defensive measure, a strategy that the clinical strain does not appear to rely on as heavily, likely due to its already optimized biofilm-related defenses.

These observations highlight the distinct proteomic strategies employed by the clinical and control strains. The clinical strain's more stable and efficient resistance mechanisms, which involve both characterized and novel proteins, contrast with the control strain's broader and more reactive defense responses. These findings suggest that the uncharacterized proteins in the clinical strain could be targets for future research aimed at uncovering novel antimicrobial resistance mechanisms and developing targeted therapies.

5 Conclusion

This study provides a comprehensive comparative analysis in *P*. aeruginosa of the proteomic responses of a clinical strain, representative of the world epidemic clone (P. aeruginosa ST235), and a control strain (P. aeruginosa ATCC 27853) to varying concentrations of imipenem. The clinical strain's ability to maintain a stable proteomic profile, even under high antibiotic pressure, underscores its reliance on pre-established resistance mechanisms. Both well-characterized and uncharacterized proteins have been found to be involved in the clinical strain's adaptation and survival. This stability contrasts sharply with the control strain's more reactive and fluctuating proteomic responses, which reflect a broad attempt to mitigate antibiotic stress. The control strain's significant proteomic shifts, particularly in proteins associated with membrane transport and stress response, highlight its less specialized and more variable approach to resistance. These findings highlight the distinct proteomic strategies employed by the clinical and control strains. The clinical strain's efficient and stable resistance mechanisms, involving both characterized and novel proteins, contrast with the control strain's broader and more reactive defense responses. The identification of uncharacterized proteins in the clinical strain as potential resistome targets for future research underscores the importance of further investigation into novel antimicrobial resistance mechanisms. This could lead to the development of targeted therapies, providing new avenues in the fight against antimicrobial resistance.

Data availability statement

The datasets presented in this study can be found in online repositories. The names of the repository/repositories and accession

number(s) can be found below: https://www.ebi.ac.uk/pride/archive/, PXD055744 (reviewer credentials in article).

Author contributions

ME: Visualization, Formal Analysis, Writing – original draft, Data curation, Investigation, Writing – review & editing, Software, Methodology. ASh: Writing – review & editing, Software, Writing – original draft, Investigation, Validation, Methodology, Data curation. MJ: Methodology, Validation, Writing – original draft, Writing – review & editing. AK: Methodology, Conceptualization, Investigation, Writing – review & editing, Writing – original draft. ASk: Writing – original draft, Methodology, Investigation, Conceptualization, Writing – review & editing. FD: Project administration, Writing – review & editing, Validation, Supervision, Methodology, Visualization, Writing – original draft, Conceptualization, Funding acquisition, Investigation.

Funding

The author(s) declare financial support was received for the research and/or publication of this article. This manuscript was developed under the project "Yeast-based biosensors for the specific and accessible detection of pathogens and antimicrobial resistance" (Acronym: AntiRYB, Reference Number: JPIAMR_2019_P08) from the Antimicrobial Resistance Joint Programming Initiative (JPI AMR) and the Research Council of Norway (RCN project number 311248). The work performed at the National Medicines Institute was funded by the National Science Centre, Poland under JPI-EC-AMR Call 2019 (NCN project number 2019/01/Y/NZ6/00006). MS-data is handled under Notur/NorStore Project NN9036K/NS9036K by PROMEC, a member of the National Network of Advanced Proteomics Infrastructure (NAPI), which is funded by the RCN INFRASTRUKTUR-program (295910).

Conflict of interest

The authors declare that the research was conducted in the absence of any commercial or financial relationships that could be construed as a potential conflict of interest.

Generative AI statement

The author(s) declare that Generative AI was used in the creation of this manuscript. During the preparation of this work the authors used ChatGPT-4 (via Microsoft Copilot) for

proofreading and suggestions for figure plotting in Python. After using this tool, the authors reviewed and edited the content as needed and take full responsibility for the content of the published article.

Any alternative text (alt text) provided alongside figures in this article has been generated by Frontiers with the support of artificial intelligence and reasonable efforts have been made to ensure accuracy, including review by the authors wherever possible. If you identify any issues, please contact us.

Publisher's note

All claims expressed in this article are solely those of the authors and do not necessarily represent those of their affiliated organizations, or those of the publisher, the editors and the reviewers. Any product that may be evaluated in this article, or claim that may be made by its manufacturer, is not guaranteed or endorsed by the publisher.

Supplementary material

The Supplementary Material for this article can be found online at: https://www.frontiersin.org/articles/10.3389/fcimb.2025.1623154/full#supplementary-material

SUPPLEMENTARY FIGURE 1

Comparative GO term enrichment in P. aeruginosa strains.

SUPPLEMENTARY FIGURE 2

Venn diagram showing the number of shared and exclusive genes among clinical and control strains.

SUPPLEMENTARY TABLE 1

List of proteins displayed in Figure 3.

SUPPLEMENTARY TABLE 2

List of proteins displayed in Figure 5.

SUPPLEMENTARY TABLE 3

Dose-correlation statistics for control strain.

SUPPLEMENTARY TABLE 4

Dose-correlation statistics for clinical strain.

SUPPLEMENTARY TABLE 5

Tabular GO-term enrichment results corresponding to Supplementary Figure S1B.

SUPPLEMENTARY TABLE 6

Tabular GO-term enrichment results corresponding to Supplementary Figure S1C.

SUPPLEMENTARY TABLE 7

Tabular GO-term enrichment results corresponding to Figure 4B.

SUPPLEMENTARY TABLE 8

List of protein IDs associated with GO terms in Table 1C.

References

(2020). ISO 20776-1:2020. Clinical laboratory testing and in vitro diagnostic test systems—Susceptibility testing of infectious agents and evaluation of performance of antimicrobial susceptibility test devices. Part 1: Broth micro-dilution reference method for testing the in vitro activity of antimicrobial agents against rapidly growing aerobic bacteria involved in infectious diseases (Geneva, Switzerland: International Organization for Standardization (ISO)).

Aslam, B., Wang, W., Arshad, M. I., Khurshid, M., Muzammil, S., Hidayat, M. R., et al. (2018). Antibiotic resistance: a rundown of a global crisis. *Infection Drug Resistance* 11, 1645–1658. doi: 10.2147/IDR.S173867

Barbier, F., Hraiech, S., Kernéis, S., Veluppillai, N., Pajot, O., Poissy, J., et al. (2023). Rationale and evidence for the use of new beta-lactam/beta-lactamase inhibitor combinations and cefiderocol in critically ill patients. *Ann. Intensive Care* 13, 65. doi: 10.1186/s13613-023-01153-6

Berrazeg, M., Jeannot, K., Ntsogo Enguéné, V. Y., Broutin, I., Loeffert, S., Fournier, D., et al. (2015). Mutations in β -lactamase ampC increase resistance of pseudomonas aeruginosa isolates to antipseudomonal cephalosporins. *Antimicrobial. Agents Chemother.* 59, 6248–6255. doi: 10.1128/AAC.00825-15

Breidenstein, E. B. M., de la Fuente-Núñez, C., and Hancock, R. E. W. (2011). Pseudomonas aeruginosa: all roads lead to resistance. *Trends Microbiol.* 19, 419–426. doi: 10.1016/j.tim.2011.04.005

Cao, H., Lai, Y., Bougouffa, S., Xu, X., and Yan, A. (2017). Comparative genome and transcriptome analysis reveals distinctive surface characteristics and unique physiological potentials of Pseudomonas aeruginosa ATCC 27853. *BMC Genomics* 18, 459. doi: 10.1186/s12864-017-3842-z

Ashburner, M., Ball, C. A., Blake, J. A., Botstein, D., Butler, H., Cherry, J. M., et al (2000). Gene ontology: tool for the unification of biology. The Gene Ontology Consortium. *Nat Genet.* 25 (1), 25–29. doi: 10.1038/75556

Cox, J., Hein, M. Y., Luber, C. A., Paron, I., Nagaraj, N., Mann, M., et al. (2014). Accurate proteome-wide label-free quantification by delayed normalization and maximal peptide ratio extraction, termed maxLFQ. *Mol. Cell. Proteomics* 13, 2513–2526. doi: 10.1074/mcp.M113.031591

Darby, E. M., Trampari, E., Siasat, P., Solsona Gaya, M., Alav, I., Webber, M. A., et al. (2023). Molecular mechanisms of antibiotic resistance revisited. *Nat. Rev. Microbiol.* 21, 280–295. doi: 10.1038/s41579-022-00820-y

Davies, J., and Davies, D. (2010). Origins and evolution of antibiotic resistance. Microbiol. Mol. Biol. reviews: MMBR 74, 417–433. doi: 10.1128/MMBR.00016-10

Dell'Anno, F., Vitale, G. A., Buonocore, C., Vitale, L., Palma Esposito, F., Coppola, D., et al. (2022). Novel insights on pyoverdine: from biosynthesis to biotechnological application. *Int. J. Mol. Sci.* 23, 11507. doi: 10.3390/ijms231911507

de Sousa, T., Silva, C., Alves, O., Costa, E., Igrejas, G., Poeta, P., et al. (2023). Determination of antimicrobial resistance and the impact of imipenem + Cilastatin synergy with tetracycline in pseudomonas aeruginosa isolates from sepsis. *Microorganisms* 11, 2687. doi: 10.3390/microorganisms11112687

Elfadadny, A., Ragab, R. F., AlHarbi, M., Badshah, F., Ibáñez-Arancibia, E., Farag, A., et al. (2024). Antimicrobial resistance of Pseudomonas aeruginosa: navigating clinical impacts, current resistance trends, and innovations in breaking therapies. *Front. Microbiol.* 15. doi: 10.3389/fmicb.2024.1374466

European Committee on Antimicrobial Susceptibility Testing (2024). Broth microdilution - EUCAST reading guide v 5.0. Available online at: https://www.eucast.org/fileadmin/src/media/PDFs/EUCAST_files/MIC_testing/Reading_guide_BMD_v_5.0_2024.pdf. (Accessed June 12, 2024).

Fair, R. J., and Tor, Y. (2014). Antibiotics and bacterial resistance in the 21st century. Perspect. Medicinal Chem. 6, 25–64. doi: 10.4137/PMC.S14459

Goodyear, M. C., Seidel, L., Krieger, J. R., Geddes-McAlister, J., Levesque, R. C., Khursigara, C. M., et al. (2023). Quantitative proteomics reveals unique responses to antimicrobial treatments in clinical *Pseudomonas aeruginosa* isolates. *mSystems* 8, e00491–e00423. doi: 10.1128/msystems.00491-23

Hashemi, M. H., Holden, B. S., Coburn, J., Taylor, M. F., Weber, S., Hilton, B., et al. (2019). Proteomic analysis of resistance of gram-negative bacteria to chlorhexidine and impacts on susceptibility to colistin, antimicrobial peptides, and ceragenins. *Front. Microbiol.* 10. doi: 10.3389/fmicb.2019.00210

Hespanhol, J. T., Nóbrega-Silva, L., and Bayer-Santos, E. (2023). Regulation of type VI secretion systems at the transcriptional, posttranscriptional and posttranslational level. *Microbiology* 169 (8), 001376. doi: 10.1099/mic.0.001376

Heywood, A., and Lamont, I. L. (2020). Cell envelope proteases and peptidases of *Pseudomonas aeruginosa*: multiple roles, multiple mechanisms. *FEMS Microbiol. Rev.* 44, 857–873. doi: 10.1093/femsre/fuaa036

Jacoby, G. A. (2009). AmpC β -lactamases. Clin. Microbiol. Rev. 22, 161–182. doi: 10.1128/CMR.00036-08

Jongers, B. S., Bielen, K., Hotterbeekx, A., Timmerman, E., Lammens, C., and Goossens, H. (2021). "Proteomic response of P. aeruginosa to sub-MIC antibiotics," in 31st European Congress of Clinical Microbiology and Infection Diseases (ECCMID). (Vienna: European Society of Clinical Microbiology and Infectious Diseases (ESCMID)).

Khodadadi, E., Zeinalzadeh, E., Taghizadeh, S., Mehramouz, B., Kamounah, F. S., Khodadadi, E., et al. (2020). Proteomic applications in antimicrobial resistance and clinical microbiology studies. *Infection Drug Resistance* 13, 1785–1806. doi: 10.2147/IDR.S238446

Langendonk, R. F., Neill, D. R., and Fothergill, J. L. (2021). The building blocks of antimicrobial resistance in pseudomonas aeruginosa: implications for current resistance-breaking therapies. *Front. Cell. Infection Microbiol.* 11. doi: 10.3389/fcimb.2021.665759

Lautenbach, E., Weiner, M. G., Nachamkin, I., Bilker, W. B., and Sheridan Fishman, A. O. N. (2006). Imipenem resistance among *pseudomonas aeruginosa* isolates risk factors for infection and impact of resistance on clinical and economic outcomes. *Infection Control Hosp. Epidemiol.* 27, 893–900. doi: 10.1086/507274

Leigue, L., Montiani-Ferreira, F., and Moore, B. A. (2016). Antimicrobial susceptibility and minimal inhibitory concentration of Pseudomonas aeruginosa isolated from septic ocular surface disease in different animal species. *Open Veterinary J.* 6, 215–222. doi: 10.4314/ovj.v6i3.9

Lewis, V. G., Ween, M. P., and McDevitt, C. A. (2012). The role of ATP-binding cassette transporters in bacterial pathogenicity. *Protoplasma* 249, 919–942. doi: 10.1007/s00709-011-0360-8

Liu, X., Pai, P., Zhang, W., Hu, Y., Dong, X., Qian, P., et al. (2016). Proteomic response of methicillin-resistant S. aureus to a synergistic antibacterial drug combination: a novel erythromycin derivative and oxacillin. *Sci. Rep.* 6, 19841. doi: 10.1038/srep19841

Mack, A. R., Hujer, A. M., Mojica, M. F., Taracila, M. A., Feldgarden, M., Haft, D. H., et al. (2025). β-Lactamase diversity in *Pseudomonas aeruginosa*. *Antimicrobial. Agents Chemother.* 69, e0078524. doi: 10.1128/aac.00785-24

Magiorakosa, A. P., Srinivasanb, A., Careyb, R. B., Carmelic, Y., Falagasde, M. E., Giskef, C. G., et al. (2012). Multidrug-resistant, extensively drug-resistant and pandrug-resistant bacteria: an international expert proposal for interim standard definitions for acquired resistance. Clin. Microbiol. Infection: Off. Publ. Eur. Soc. Clin. Microbiol. Infect. Dis. 18, 268–281. doi: 10.1111/j.1469-0691.2011.03570.x

Matilla, M. A., Udaondo, Z., Maaß, S., Becher, D., and Krell, T. (2022). Virulence Induction in Pseudomonas aeruginosa under Inorganic Phosphate Limitation: a Proteomics Perspective. *Microbiol. Spectr.* 10, e02590–e02522. doi: 10.1128/spectrum.02590-22

Mosquera-Rendón, J., Rada-Bravo, A. M., Cárdenas-Brito, S., Corredor, M., Restrepo-Pineda, E., Benítez-Páez, A., et al. (2016). Pangenome-wide and molecular evolution analyses of the Pseudomonas aeruginosa species. *BMC Genomics* 17, 45. doi: 10.1186/s12864-016-2364-4

Oliver, A., Mulet, X., López-Causapé, C., and Juan, C. (2015). The increasing threat of Pseudomonas aeruginosa high-risk clones. *Drug Resistance Updates: Rev. Commentaries Antimicrobial. Anticancer Chemother.* 21-22, 41–59. doi: 10.1016/j.drup.2015.08.002

Pérez-Llarena, F. J., and Bou, G. (2016). Proteomics as a tool for studying bacterial virulence and antimicrobial resistance. *Front. Microbiol.* 7. doi: 10.3389/fmicb.2016.00410

Perez-Riverol, Y., Bai, J., Bandla, C., García-Seisdedos, D., Hewapathirana, S., Kamatchinathan, S., et al. (2022). The PRIDE database resources in 2022: a hub for mass spectrometry-based proteomics evidences. *Nucleic Acids Res.* 50, D543–D552. doi: 10.1093/nar/gkab1038

Sulaiman, J. E., and Lam, H. (2022). Proteomics in antibiotic resistance and tolerance research: Mapping the resistome and the tolerome of bacterial pathogens. *Proteomics* 22, e2100409. doi: 10.1002/pmic.202100409

Treepong, P., Kos, V. N., Guyeux, C., Blanc, D. S., Bertrand, X., Valot, B., et al. (2018). Global emergence of the widespread Pseudomonas aeruginosa ST235 clone. *Clin. Microbiol. Infection* 24, 258–266. doi: 10.1016/j.cmi.2017.06.018

Tyanova, S., Temu, T., and Cox, J. (2016). The MaxQuant computational platform for mass spectrometry-based shotgun proteomics. *Nat. Protoc.* 11, 2301–2319. doi: 10.1038/nprot.2016.136

UniProt Consortium (2022). Pseudomonas aeruginosa (strain PAO1) reference proteome. Available online at: https://www.uniprot.org/proteomes/UP000002438. (Accessed March 08, 2024).

Uni
Prot Consortium (2023). Uni Prot: the universal protein knowledge
base in 2023. Nucleic Acids Res. 51, D523–D531. doi: 10.1093/nar/gkac
1052

Urbanowicz, P., Izdebski, R., Baraniak, A., Żabicka, D., Hryniewicz, W., Gniadkowski, M., et al. (2021). Molecular and genomic epidemiology of VIM/IMP-like metallo- β -lactamase-producing *Pseudomonas aeruginosa* genotypes in Poland. *J. Antimicrobial. Chemother.* 76, 2273–2284. doi: 10.1093/jac/dkab188

Wright, G. D. (2007). The antibiotic resistome: the nexus of chemical and genetic diversity. *Nat. Rev. Microbiol.* 5, 175–186. doi: 10.1038/nrmicro1614

Xu, Y., Zheng, X., Zeng, W., Chen, T., Liao, W., Qian, J., et al. (2020). Mechanisms of heteroresistance and resistance to imipenem in pseudomonas aeruginosa. *Infection Drug Resistance* 13, 1419–1428. doi: 10.2147/IDR.S249475

Young, K., Painter, R. E., Raghoobar, S. L., Hairston, N. N., Racine, F., Wisniewski, D., et al. (2019). *In vitro* studies evaluating the activity of imipenem in combination with relebactam against Pseudomonas aeruginosa. *BMC Microbiol.* 19, 150. doi: 10.1186/s12866-019-1522-7

Zhao, G., He, F., Wu, C., Li, P., Li, N., Deng, J., et al. (2018). Betaine in inflammation: mechanistic aspects and applications. *Front. Immunol.* 9. doi: 10.3389/fimmu.2018.01070